2024 European Control Conference (ECC)
June 25-28, 2024. Stockholm, Sweden

Posture estimation for a high degree of freedom anthropomorphic tendon-based hand model – A simulation experiment*

Péter Polcz[1], Katalin Schäffer[1,2], and Miklós Koller[1].

***Abstract*— Tendon-based anthropomorphic robotic hand implementations generally lack the ability to measure the joint angles, as the encoder installed for directly measuring the joint angle may compromise the dexterity of the hand. In this paper, we present a computational approach to estimate the joint positions of the hand using the measured tendon displacements and tensions. First, we introduce an efficient framework for the kinematic description of an anthropomorphic hand based on Denavit-Hartenberg's description. Then, we use a simplified tendon model to derive a system of nonlinear equations for the joint positions, which is finally solved by a gradient-based optimization solver. We used the model to control the hand along commanded gestures by feeding back the estimated joint angles through the moment arm Jacobian. The effectiveness and limitations of this method is illustrated in MuJoCo simulation environment on the Anatomically Correct Biomechatronic Hand having a 5 and 6 degrees of freedom kinematic models for the long fingers and the thumb, respectively.**

***Index Terms*— Biomechatronic hand, tendon-based actuation, posture estimation, Denavit-Hartenberg**

I. Introduction

In robotics, it is still a challenge to develop anthropomorphic hand models that can imitate the dexterity of the human hand. A commonly used approach to achieve better biological accuracy is to mimic the entire biological structure of the hand, including the tendon-based actuation mechanism of the hand [1]–[8].

In particular, the Anatomically Correct Biomechatronic (ACB) Hand developed by Tasi et al. [8] precisely follows the shapes and structures of a human hand to mimic human hand's dexterity as much as possible. In such robotics systems the bones of the fingers can be displaced along more degrees of freedom compared to the segments of a conventional robotic manipulator. Differently from [5]–[7], the metacarpals of long fingers in [8], for example, can rotate about all the three axes (Pitch, Yaw, and Roll). For such models, even kinematic description is difficult using the Denavit-Hartenberg (DH) convention, see, e.g., [9], [10].

Needless to say that the precise knowledge of the joint posture is essential for control algorithms [11], [12], [13]. However, as encoder installed to the (possibly multiple DoF) joints would compromise the mobility of the hand, the joint angles are generally not measured but estimated, e.g., from the tendon excursions using feedforward neural networks [14] or through motion capture [15]. As demonstrated in [16], joint coupling also allows exact gesture computation from tendon excursions, but it significantly reduces the manipulators functionality compared to a human hand.

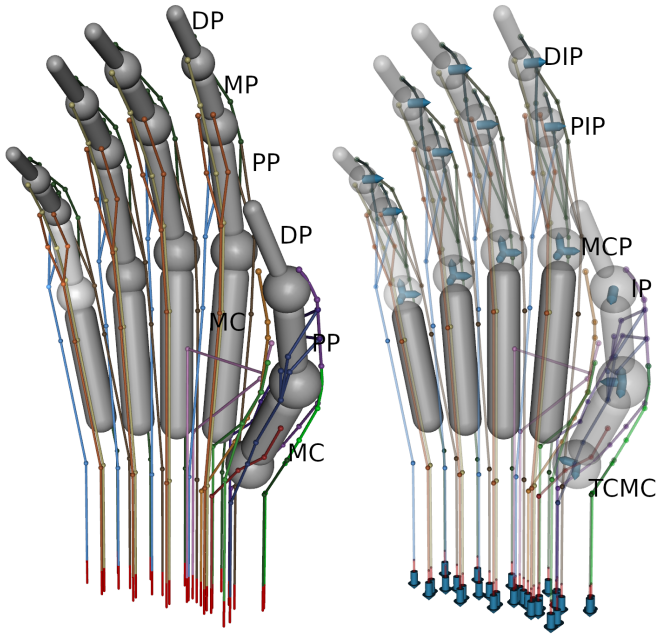

Fig. 1. Bone structure of the ACB Hand at rest position. Abbreviations of the bones are given in the left figure, whereas, the right figure illustrate the joints with their names, and their degrees of freedom (i.e., the axes of free rotations).

The major contribution of this paper is a joint posture estimation method for the ACB Hand model by solving a system of nonlinear equations. Additionally, we propose a systematic Denavit-Hartenberg's (DH) description for finger-type manipulators where the links are connected irregularly by 3 degrees of freedom (DoF) joints. Our approach is not a data-based machine learning solution, but an analytical method, iteratively improving the estimates and the control values. As a benefit, in this case the cause-and-effect relationships can be identified (eg. as it helped us in the tendon placement optimization on the in-silico model), the whole control process is more humanly understandable. On contrary, as a limitation we can see that not all of the gestures and gesture-transients can be tackled seamlessly. For such high-dimensional problems the data-driven solutions could be more powerful, apart from their black-box nature.

II. Compute joint angles and excursion of connected tendon segments

A. Bone structure and its kinematic model

In this paper, we follow the bone structure developed by Tasi et al. [8], where the bones are connected by 1,

*Project no. TKP2021-NKTA-66 has been implemented with the support provided by the Ministry of Technology and Industry of Hungary from the National Research, Development and Innovation Fund, financed under the TKP2021-NKTA funding scheme.

[1]Authors are with Faculty of Information Technology and Bionics, Pázmány Péter Catholic University, Budapest, Hungary, (e-mail: polcz.peter|schaffer.katalin|koller.miklos@itk.ppke.hu)

[2]K. Schäffer is also with the Department of Aerospace and Mechanical Engineering, University of Notre Dame, Notre Dame, IN 46556, USA (e-mail: kschaff2@nd.edu.

2, or 3 DoF joints. The flexion-extension is described by Pitch rotation, adduction-abduction is the Yaw rotation, and the pronation-supination is given by Roll rotation. The metacarpophalangeal (MCP) joints of ACB Hand has 3 DoF, allowing the proximal phalanges (PP) to be displaced in both Pitch, Yaw and Roll directions. The thumb carpometacarpal (TCMC) joint has 2 DoF, thus the metacarpal (MC) of the thumb can freely rotate about both Pitch and Yaw axes. The proximal interphalangeal (PIP), distal interphalangeal (DIP) joints, and the interphalangeal (IP) of the thumb have a free hinge motion only about the Pitch axis. The bone structure is illustrated in Figure 1.

The irregular alignment of the cartilages causes two bones to deflect and twist relative to each other (even in the rest position). These irregularities are modeled by offset angles. The deflection is described Pitch and Yaw offsets, whereas, the twist is given by the Roll offset.

In our geometric model, the bone structure is built such that the alignment of two bones can be described by six angles: three fixed offset angles and the rotations about the three free joints. One possible way to construct a DH table for such robotic manipulators with n links and 3-DoF joints is given in Table I, where $(X_\mathrm{o}, Y_\mathrm{o}, Z_\mathrm{o})$ is the coordinate of the first joint and L_k is the length of the kth link. This convention allows the removal of the appropriate pair of $(3j, 3j+1)$ rows when a Yaw rotation is missing, e.g., when Joint 1 Yaw vanishes, rows $(3, 4)$ are negligible. Using the presented convention, the DH tables of a long finger and the thumb are given in Tables II and III, respectively.

B. Tendon structure

For simplicity, we discuss only the index finger, which is manipulated by $n_\mathrm{m} = 5$ muscles, namely, flexor digitorium superficialis (FDS), flexor digitorium profundus (FDP), extensor digitorium communis (EDC), lumbrical (LUM), and ulnar interosseous (UI). Tendons EDC, UI, and LUM are divided, then, connected again such that they form two lateral bands (LBs), the extensor slip (ES), and the terminal extensor (TE). We note that this tendon structure corresponds to that presented in [11] and is a simplified version of [8].

As illustrated in Figure 2, the tendon structure of the index finger is described by a directed acyclic graph having three types of vertices: starting sites (V_m), junctions (V_j), and terminal sites (V_bn). A starting site is connected to a muscle, whereas, a terminal site is fixed to a bone. The number of edges starting from a vertex v is called the out-degree of the vertex and is denoted by $\mathrm{d}_-(v)$. Similarly, $\mathrm{d}_+(v)$ denotes the number of edges arriving to vertex v and is called the in-degree if v. A tendon segment is a directed edge of the graph, which connects two vertices in four possible ways:

- a starting site with a terminal site ($v_\mathrm{m} \to v_\mathrm{bn}$),
- a starting site with a junction ($v_\mathrm{m} \to v_\mathrm{j}$),
- a junction with a terminal site ($v_\mathrm{j} \to v_\mathrm{bn}$),
- a junction with a junction ($v_\mathrm{j} \to v'_\mathrm{j}$),

such that every starting ($v_\mathrm{m} \in V_\mathrm{m}$) and terminal sites ($v_\mathrm{bn} \in V_\mathrm{bn}$) and junctions ($v_\mathrm{j} \in V_\mathrm{j}$) satisfy the following

$$\begin{aligned} &\mathrm{d}_+(v_\mathrm{m}) = 0, \quad \mathrm{d}_-(v_\mathrm{m}) = 1, \\ &\mathrm{d}_+(v_\mathrm{bn}) = 1, \quad \mathrm{d}_-(v_\mathrm{bn}) = 0, \\ &\min\left(\mathrm{d}_+(v_\mathrm{j}), \mathrm{d}_-(v_\mathrm{j})\right) \geq 1, \\ &\max\left(\mathrm{d}_+(v_\mathrm{j}), \mathrm{d}_-(v_\mathrm{j})\right) \geq 2. \end{aligned} \tag{1}$$

i	d	ϑ	a	α
	Z_o	0	X_o	-90°
	Y_o	-90°	0	*Joint* 1 *Roll Offset*
1	0	*Joint* 1 *Yaw Offset*	0	-90°
2	0	*Joint* 1 *Pitch Offset*	0	**Joint** 1 **Roll**
3	0	0	0	90°
4	0	**Joint** 1 **Yaw**	0	-90°
5	0	**Joint** 1 **Pitch**	L_1	*Joint* 2 *Roll Offset*
6	0	0	0	90°
...		...		...
$6k-5$	0	*Joint* k *Yaw Offset*	0	-90°
$6k-4$	0	*Joint* k *Pitch Offset*	0	**Joint** k **Roll**
$6k-3$	0	0	0	90°
$6k-2$	0	**Joint** k **Yaw**	0	-90°
$6k-1$	0	**Joint** k **Pitch**	L_k	*Joint* $k+1$ *Roll Offset*
$6k$	0	0	0	90°
...		...		...
$6n-2$	0	**Joint** n **Yaw**	0	-90°
$6n-1$	0	**Joint** n **Pitch**	L_n	0

TABLE I

DH TABLE FOR A MANIPULATOR WITH n LINKS CONNECTED IRREGULARLY THROUGH 3-DOF ROTARY JOINTS

i	d	ϑ	a	α
	Z_o	0	X_o	-90°
	Y_o	-90°	0	*CMC Roll offset*
1	0	*CMC Yaw offset*	0	-90°
2	0	*CMC Pitch offset*	L_MC	*MCP Roll offset*
6	0	0	0	90°
7	0	*MCP Yaw offset*	0	-90°
8	0	*MCP Pitch offset*	0	**MCP Roll**
9	0	0	0	90°
10	0	**MCP Yaw**	0	-90°
11	0	**MCP Pitch**	L_PP	*PIP Roll offset**
14	0	*PIP Pitch offset*	0	0
17	0	**PIP Pitch**	L_MP	*DIP Roll offset**
20	0	*DIP Pitch offset*	0	0
23	0	**DIP Pitch**	L_DP	0

*PIP and DIP Yaw offsets are missing

TABLE II

DH TABLE OF THE 5 DOF LONG FINGERS OF ACB HAND.

i	d	ϑ	a	α
	Z_o	0	X_o	-90°
	Y_o	-90°	0	*TCMC Roll Offset*
1	0	*TCMC Yaw Offset*	0	-90°
2	0	*TCMC Pitch Offset*	0	90°
4	0	**TCMC Yaw**	0	-90°
5	0	**TCMC Pitch**	L_MC	*MCP Roll Offset**
8	0	*MCP Pitch Offset*	0	**MCP Roll**
9	0	0	0	90°
10	0	**MCP Yaw**	0	-90°
11	0	**MCP Pitch**	L_PP	*IP Roll Offset**
14	0	*IP Pitch Offset*	0	0
17	0	**IP Pitch**	L_DP	0

*Yaw offsets are missing at the thumb's MCP and IP joints

TABLE III

DH TABLE FOR THE 6 DOF THUMB FINGER OF ACB HAND.

In the last condition, we assumed that every junction has at least one degree (in- or out-) greater than 1. Otherwise, the trivial junction can be omitted such that the tendon segment arriving to the junction can be merged to the segment starting from the junction.

A root segment is a tendon segment connected directly to a muscle through a starting site (v_{m}). Let n_{m} denote the number of root segments and n_{ct} the number of tendon segments connected to other tendons. The overall number of tendon segments is $n_{\mathrm{s}} = n_{\mathrm{m}} + n_{\mathrm{ct}}$. The ordinal numbering of tendon segments is such that the first n_{m} segments are roots, followed by n_{ct} connected segments.

A tendon branch is a sequence of segments connecting a starting site v_{m} and a terminal site v_{bn}, i.e., connecting a muscle with a bone, see, e.g., branch (4) – (10) – (15) – (18) in Figure 2. The number of tendon branches (n_{b}) can be counted as follows:

$$n_{\mathrm{b}} = n_{\mathrm{m}} + \sum_{i=1}^{n_{\mathrm{j}}} \big(d_{+}(v_{\mathrm{j},i}) - 1\big) = n_{\mathrm{m}} - n_{\mathrm{j}} + \underbrace{\sum_{i=1}^{n_{\mathrm{j}}} d_{+}(v_{\mathrm{j},i})}_{n_{\mathrm{ct}}}. \tag{2}$$

One may observe that the sum of out degrees of junctions correspond to the number of connected tendons n_{ct}. This fact is already anticipated in (2). Finally, we may conclude that the number of junctions together with the number of branches are equal to the number of tendon segments, formally:

$$n_{\mathrm{b}} + n_{\mathrm{j}} = n_{\mathrm{m}} + n_{\mathrm{ct}} = n_{\mathrm{s}}. \tag{3}$$

The $n_{\mathrm{m}} = 5$ tendons of the long fingers have $n_{\mathrm{b}} = 10$ branches (B0–B9) in total:

$$\begin{aligned}
&\text{FDP: } (1) && \text{[B0]}\\
&\text{FDS: } (2) - \begin{cases}(6) & \text{[B1]}\\ (7) & \text{[B2]}\end{cases}\\
&\text{UI: } (3) - \begin{cases}(8) - (15) - (18) & \text{[B3]}\\ (9) - (16) & \text{[B4]}\end{cases}\\
&\text{EDC: } (4) - \begin{cases}(10) - (15) - (18) & \text{[B5]}\\ (11) - (16) & \text{[B6]}\\ (12) - (17) - (18) & \text{[B7]}\end{cases}\\
&\text{LUM: } (5) - \begin{cases}(13) - (16) & \text{[B8]}\\ (14) - (17) - (18) & \text{[B9]}\end{cases}
\end{aligned} \tag{4}$$

III. Posture Estimation from Tendon Excursion

A. Preliminaries

The index finger has $n_\theta = 5$ free joints (MCP Roll, MCP Yaw, MCP Pitch, PIP Pitch, and DIP Pitch). The angles of free joints are collected in a vector $\theta \in \mathbb{R}^{n_\theta}$. Let $\theta_0 \in \mathbb{R}^{n_\theta}$ denote the angles corresponding to the equilibrium position when all tendons are relaxed. It is reasonable to assume that that an any admissible gesture of the finger can be uniquely determined by a vector of joint angles θ. However, we do not expect that a tendon excursions pattern uniquely determines a posture and vice-versa. Nevertheless, a simple kinematic model allows us to compute the length of the piecewise straight tendons passing through some well-define site points, which fixed relative to the bones.

Let $L_{\mathrm{s},i}(\theta)$ denotes the gesture-dependent length of tendon segment $i \in \{1, \dots, n_{\mathrm{s}}\}$ (e.g., segments 1–18 in Figure 2, $n_{\mathrm{s}} = 18$). The length of a segment is calculated by the Euclidean distance between its constituent site points. When a tendon bypasses the joint around the longer arch, the segment is complemented with two auxiliary site points to approximate the curve of the tendon with a piecewise straight tendon structure. $L_{\mathrm{s}0,i} = L_{\mathrm{s},i}(\theta_0)$ denotes the length of the ith segment in the equilibrium position. The excursion of the ith segment is denoted by $\ell_{\mathrm{s},i}(\theta)$. The acting tension along the ith segment is $f_{\mathrm{s},i} = k_i\, \ell_{\mathrm{s},i}$, where $k_i = \frac{E \cdot A}{L_{\mathrm{s}0,i}}$ is the spring (or stiffness) coefficient, E is Young's (tensile) elastic modulus, and A is the cross section area of the tendon. Then,

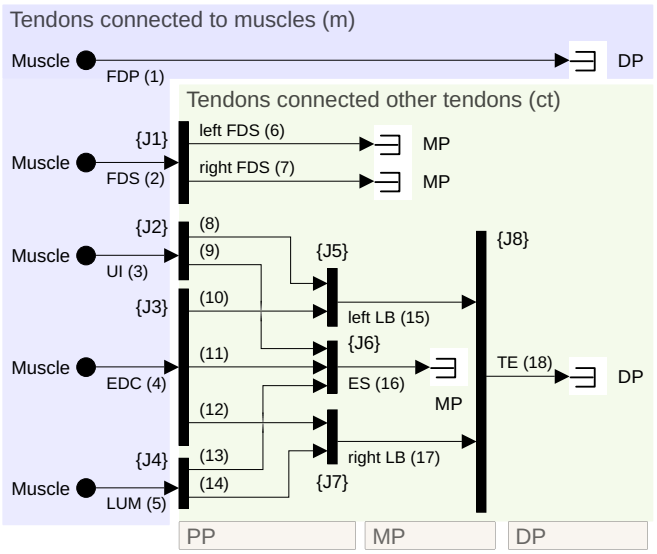

Fig. 2. Tendon structure of the index finger

$$L_{\mathrm{s}}(\theta) = \begin{pmatrix} L_{\mathrm{m}}(\theta) \\ L_{\mathrm{ct}}(\theta) \end{pmatrix} = \left(\begin{array}{c} L_{\mathrm{s},1}(\theta) \\ \dots \\ L_{\mathrm{s},n_{\mathrm{m}}}(\theta) \\ \hline L_{\mathrm{s},n_{\mathrm{m}}+1}(\theta) \\ \dots \\ L_{\mathrm{s},n_{\mathrm{m}}+n_{\mathrm{ct}}}(\theta) \end{array}\right),$$

similarily

$$\ell_{\mathrm{s}}(\theta) = \begin{pmatrix} \ell_{\mathrm{m}}(\theta) \\ \ell_{\mathrm{ct}}(\theta) \end{pmatrix}, \quad \text{or} \quad f_{\mathrm{s}} = \begin{pmatrix} f_{\mathrm{m}} \\ f_{\mathrm{ct}} \end{pmatrix}.$$

Let $\Delta L_{\mathrm{m},i}$ denote the length of stretched tendon segment coiled on the motor shaft, $i \in \{1, \dots, n_{\mathrm{m}}\}$. When $\Delta L_{\mathrm{m},i}$ is positive, tendon i is coiled up on the shaft, whereas a negative $\Delta L_{\mathrm{m},i}$ means that tendon is coiled down relative to the equilibrium length.

B. Excursion from tendon structure model

In the knowledge of the joint angles $\theta \in \mathbb{R}^{n_\theta}$, we are able to approximate the length of each tendon segment with the assumption that the site points and junctions are fixed relative to the bones of the finger. Let $L_{\mathrm{s}} : \mathbb{R}^{n_\theta} \to \mathbb{R}^{n_{\mathrm{s}}}$ denote this mapping, such that $L_{\mathrm{s},i}(\theta)$ denotes the gesture-dependent length of the ith segment, $i \in \{1, \dots, n_{\mathrm{s}}\}$. During the model description, the junctions were positioned relatively to the bones in the equilibrium position of the fingers represented by angles θ_0, therefore, the length of tendon segments $L_{\mathrm{s}0} = L_{\mathrm{s}}(\theta_0)$ in the equilibrium position well approximates

the actual lengths of tendons of the physical robotic hand prosthesis.

The length of tendon branches $L_{\mathrm{b}}(\theta)$ in an arbitrary gesture (θ) can be computed by the sum of the appropriate tendon segments as follows:

$$L_{\mathrm{b}}(\theta) = C_{\mathrm{b,s}}\, L_{\mathrm{s}}(\theta), \tag{5}$$

in particular

$$L_{\mathrm{b0}} = C_{\mathrm{b,s}}\, L_{\mathrm{s0}} = C_{\mathrm{b,s}}\, L_{\mathrm{s}}(\theta_0), \tag{6}$$

where $C_{\mathrm{b,s}} \in \mathbb{R}^{n_{\mathrm{b}} \times n_{\mathrm{s}}}$ is a sparse matrix, in which the (i,j)th element is 1 if the ith branch contains the jth segment and 0 otherwise. The actual value of $C_{\mathrm{b,s}}$ for the long fingers is given as follows:

$$\begin{array}{c|ccccc|ccccccccccccc}
 & f_1 & f_2 & f_3 & f_4 & f_5 & f_6 & f_7 & f_8 & f_9 & f_{10} & f_{11} & f_{12} & f_{13} & f_{14} & f_{15} & f_{16} & f_{17} & f_{18} \\
\hline
\mathrm{J1} & 0 & -1 & 0 & 0 & 0 & 1 & 1 & 0 & 0 & 0 & 0 & 0 & 0 & 0 & 0 & 0 & 0 & 0 \\
\mathrm{J2} & 0 & 0 & -1 & 0 & 0 & 0 & 0 & 1 & 1 & 0 & 0 & 0 & 0 & 0 & 0 & 0 & 0 & 0 \\
\mathrm{J3} & 0 & 0 & 0 & -1 & 0 & 0 & 0 & 0 & 0 & 1 & 1 & 1 & 0 & 0 & 0 & 0 & 0 & 0 \\
\mathrm{J4} & 0 & 0 & 0 & 0 & -1 & 0 & 0 & 0 & 0 & 0 & 0 & 0 & 1 & 1 & 0 & 0 & 0 & 0 \\
\mathrm{J5} & 0 & 0 & 0 & 0 & 0 & 0 & 0 & -1 & 0 & -1 & 0 & 0 & 0 & 0 & 1 & 0 & 0 & 0 \\
\mathrm{J6} & 0 & 0 & 0 & 0 & 0 & 0 & 0 & 0 & -1 & 0 & -1 & 0 & -1 & 0 & 0 & 1 & 0 & 0 \\
\mathrm{J7} & 0 & 0 & 0 & 0 & 0 & 0 & 0 & 0 & 0 & 0 & 0 & -1 & 0 & -1 & 0 & 0 & 1 & 0 \\
\mathrm{J8} & 0 & 0 & 0 & 0 & 0 & 0 & 0 & 0 & 0 & 0 & 0 & 0 & 0 & 0 & -1 & 0 & -1 & 1
\end{array}$$

$$= C_{\mathrm{j,s}} = (C_{\mathrm{j,m}} \quad C_{\mathrm{j,ct}}) \in \mathbb{R}^{n_{\mathrm{j}} \times n_{\mathrm{s}}}. \tag{7}$$

Remark 1: Although the length of segments are computed for junctions fixed to the bones, this modeling error is vanishingly small in $L_{\mathrm{b}}(\theta)$ as the length of segments are accumulated along a tendon branch.

C. Measured or preliminarily available variables

First of all, the tensions $f_{\mathrm{m}} \in \mathbb{R}^{n_{\mathrm{m}}}$ acting in tendons directly connected to the muscles can be obtained from the servo motor armature current, or by using custom tension sensors, e.g., [14]. Secondly, the lengths of tendon segments $\Delta L_{\mathrm{m}} \in \mathbb{R}^{n_{\mathrm{m}}}$ coiled on the motor shaft can be inferred from the servo motor's encoder. Whereas, Young's modulus E, the cross section area A, and hence the spring coefficients $k_i = \frac{E \cdot A}{L_{\mathrm{s0},i}}$ of the tendon segments can be measured apriori, $i \in \{1, \ldots, n_{\mathrm{s}}\}$.

D. Unknown variables

Since no encoder are mounted in the finger joints, the angles $\theta \in \mathbb{R}^{n_\theta}$ of the free joints are all unknown. Moreover, the actual excursion $\ell_{\mathrm{ct}} \in \mathbb{R}^{n_{\mathrm{ct}}}$, and hence the acting tensions $f_{\mathrm{ct}} = K_{\mathrm{ct}} \ell_{\mathrm{ct}}$ in the connected tendons are unknown. Diagonal matrix K_{ct} contains the spring coefficients of the connected tendon segments, i.e., $K_{\mathrm{ct}} = \mathrm{diag}(k_{n_{\mathrm{m}}+1}, \ldots, k_{n_{\mathrm{m}}+n_{\mathrm{ct}}})$.

E. Dependent variables

Our model allows to compute the total excursion of a tendon branch in two different ways. First, we can infer it from the excursions of individual segments, which form the branch, namely:

$$\ell_{\mathrm{b}} = C_{\mathrm{b,s}} \ell_{\mathrm{s}} = C_{\mathrm{b,m}} \ell_{\mathrm{m}} + C_{\mathrm{b,ct}} \ell_{\mathrm{ct}}. \tag{8}$$

Secondly, the fixed-site geometric tendon model makes it possible to compute the total length, and hence the excursion of a branch from the gesture of the hand as follows:

$$\underbrace{L_{\mathrm{b}}(\theta) + \Delta L_{\mathrm{b}}}_{\text{stretched length of the branch}} - \overbrace{L_{\mathrm{b0}}}^{\text{unstretched length of the branch}} = \underbrace{\ell_{\mathrm{b}}}_{\text{total excursion along the branch}} \tag{9}$$

Then, an equation from (8) and (9) can be obtained as follows:

$$L_{\mathrm{b}}(\theta) + C_{\mathrm{b,m}}\, \Delta L_{\mathrm{m}} - L_{\mathrm{b0}} = C_{\mathrm{b,m}}\, \underbrace{K_{\mathrm{m}}^{-1}\, f_{\mathrm{m}}}_{\ell_{\mathrm{m}}} + C_{\mathrm{b,ct}}\, \ell_{\mathrm{ct}}. \tag{10}$$

Finally, we exploit the fact that the acting forces in a junction cancel each other out. E.g., in Figure 2, forces f_2, f_6, and f_7 acting in junction {J1} must satisfy $f_2 = f_6 + f_7$. These conditions can be described by the following equation:

$$C_{\mathrm{j,s}}\, f_{\mathrm{s}} = C_{\mathrm{j,m}}\, f_{\mathrm{m}} + C_{\mathrm{j,ct}}\, K_{\mathrm{ct}} \ell_{\mathrm{ct}} = 0, \tag{11}$$

where $C_{\mathrm{j,s}}$ represents the connection matrix of tendon junctions. The (i,j)th element of $C_{\mathrm{j,s}}$ is -1 if segment j enters junction i, $+1$ if it leaves, and 0 if they are not connected. At this point we assumed that all forces arising at a junction act along the same line, namely, the angle between every two force vectors are 0 or π. The actual value of $C_{\mathrm{j,s}}$ for the long fingers is

$$\begin{array}{c|ccccc|ccccccccccccc}
 & \ell_1 & \ell_2 & \ell_3 & \ell_4 & \ell_5 & \ell_6 & \ell_7 & \ell_8 & \ell_9 & \ell_{10} & \ell_{11} & \ell_{12} & \ell_{13} & \ell_{14} & \ell_{15} & \ell_{16} & \ell_{17} & \ell_{18} \\
\hline
\mathrm{B0} & 1 & 0 & 0 & 0 & 0 & 0 & 0 & 0 & 0 & 0 & 0 & 0 & 0 & 0 & 0 & 0 & 0 & 0 \\
\mathrm{B1} & 0 & 1 & 0 & 0 & 0 & 1 & 0 & 0 & 0 & 0 & 0 & 0 & 0 & 0 & 0 & 0 & 0 & 0 \\
\mathrm{B2} & 0 & 1 & 0 & 0 & 0 & 0 & 1 & 0 & 0 & 0 & 0 & 0 & 0 & 0 & 0 & 0 & 0 & 0 \\
\mathrm{B3} & 0 & 0 & 1 & 0 & 0 & 0 & 0 & 1 & 0 & 0 & 0 & 0 & 0 & 0 & 1 & 0 & 0 & 1 \\
\mathrm{B4} & 0 & 0 & 1 & 0 & 0 & 0 & 0 & 0 & 1 & 0 & 0 & 0 & 0 & 0 & 0 & 1 & 0 & 0 \\
\mathrm{B5} & 0 & 0 & 0 & 1 & 0 & 0 & 0 & 0 & 0 & 1 & 0 & 0 & 0 & 0 & 1 & 0 & 0 & 1 \\
\mathrm{B6} & 0 & 0 & 0 & 1 & 0 & 0 & 0 & 0 & 0 & 0 & 1 & 0 & 0 & 0 & 0 & 1 & 0 & 0 \\
\mathrm{B7} & 0 & 0 & 0 & 1 & 0 & 0 & 0 & 0 & 0 & 0 & 0 & 1 & 0 & 0 & 0 & 0 & 1 & 1 \\
\mathrm{B8} & 0 & 0 & 0 & 0 & 1 & 0 & 0 & 0 & 0 & 0 & 0 & 0 & 1 & 0 & 0 & 1 & 0 & 0 \\
\mathrm{B9} & 0 & 0 & 0 & 0 & 1 & 0 & 0 & 0 & 0 & 0 & 0 & 0 & 0 & 1 & 0 & 0 & 1 & 1
\end{array}$$

$$= C_{\mathrm{b,s}} = (C_{\mathrm{b,m}} \quad C_{\mathrm{b,ct}}) \in \mathbb{R}^{n_{\mathrm{j}} \times n_{\mathrm{s}}}. \tag{12}$$

It is worth mentioning that the number of equations in (10) and (11) are n_{b} and n_{j}, respectively. Whereas, the number of unknown variables is $n_\theta + n_{\mathrm{ct}}$. Moreover, it is reasonable to assume that the number of muscle actuators (n_{m}) of a finger is at least equal to the number of free joints n_θ, i.e.,

$$n_\theta \leq n_{\mathrm{m}}. \tag{13}$$

If we add $n_{\mathrm{ct}} = n_{\mathrm{s}} - n_{\mathrm{m}} = n_{\mathrm{b}} + n_{\mathrm{j}} - n_{\mathrm{m}}$ to both sides of inequality (13), we obtain

$$n_\theta + n_{\mathrm{ct}} \leq n_{\mathrm{b}} + n_{\mathrm{j}}. \tag{14}$$

Finally, we can conclude that the number of equations in (10) and (11) is at least the number of unknown with the assumption that $n_\theta \leq n_{\mathrm{m}}$.

IV. Simulation Experiment

Here, we evaluate a simple posture tracking controller, in which the error between the desired position $\theta^{(\mathrm{d})}$ and the estimated position $\hat{\theta}$ is fed back through the Jacobian matrix. The experiment is performed in MuJoCo simulation environment [17], in which the tendon length is computed as the average length of tendon branches. The branches of the tendons were give previously in (4). In MuJoCo's modelling language, junctions {J5}–{J8} are neglected such that the tendons LB, ES, ET are composed of the independent

branches of EDC, UI, and LUM.

Let $L_{\mathrm{m}} : \mathbb{R}^{n_\theta} \to \mathbb{R}^{n_{\mathrm{m}}}$ denote the length of the tendons, and consider its Jacobian matrix:

$$R_{\mathrm{m}}(\theta) = \frac{\partial L_{\mathrm{m}}}{\partial \theta}(\theta) \in \mathbb{R}^{n_{\mathrm{m}} \times n_\theta}. \tag{15}$$

The actuation level is then computed by the displacement of the starting site of the root segment, which is connected directly to the shaft of the servo motor. In a given time step, the displacement of the starting site is modified as follows:

$$\Delta L_{\mathrm{m}}^{+} = \Delta L_{\mathrm{m}} - R_{\mathrm{m}}(\theta)\left(K_{\mathrm{P}}\,\tilde{\theta} + K_{\mathrm{I}} \textstyle\sum_k h\,\tilde{\theta}(k)\right), \tag{16}$$

where $\tilde{\theta} = \hat{\theta} - \theta^{(\mathrm{d})}$ is the tracking error, h is the sampling time, $\Delta L_{\mathrm{m}}^{+}$ denotes the length of tendon coiled on the shaft in the next time step. The summation term in (16) constitutes the cumulative error feedback, which together with the proportial feedback realize a proportional-integral (PI) controller. In computations, we used $K_{\mathrm{P}} = 0.7$, $K_{\mathrm{I}} = 0.1$.

To solve (10) and (11), we executed a constrained gradient-based search without a cost function. For algorithmic differentiation, we used CasADi [18]. To solve the non-linear feasibility problem, we used IPOPT [19], an interior point line search algorithm, with the MUlti-frontal Massively Parallel sparse direct Solver (MUMPS) [20], [21]. The MuJoCo simulation was executed at 500 Hz, whereas, the posture estimation with IPOPT lasts about 10-15 milliseconds. Therefore, the posture observation was updated at about 50 Hz.

In Figure 3, we illustrate several desired gestures achieved sequentially, where the first gesture must be reached from the resting position, and each subsequent position is attained from the previous one. Finally, the hand is directed back to the resting position. In all panels (G1)–(G6) in Figure 3 the red transparent bodies illustrate the desired gesture, the yellow transparent bodies highlight the estimated gestures, and the gray solid bodies show the actual position of the hand. In Figure 4, we present the time functions of the actual and observed angle positions together with the range of the angles.

The inaccurate estimation in (G5) can be attributed to the fingers colliding during fist clenching. At this gesture, a few joint angles of the simulated hand, goes to the infeasible region (dashed red area), which may be due to the soft implementation of constraints in MuJoCo [22]. One may observe further observation errors in Roll angle estimation in Plots 6 and 11. Based on the authors' experience, the MPC Roll angles are difficult to estimate with the current tendon structure. Nevertheless, it is noteworthy that the lengths of the feasible intervals for the MPC Roll angles are only 3 to 13 degrees.

Another unusual event took place at (G4) in Plot 11, when the actual Roll angle is closer to the reference than the estimated value. But it is also evident that the angle did not change compared to (G3). In the case of the gesture (G4), the method did not precisely compute the MPC Roll value, nonetheless, the relatively small difference between the observed and actual angles is insufficient to significantly alter the deviation from the reference in the given time window.

The results suggest that, except for the Roll angles and during collision events, the method demonstrates favorable

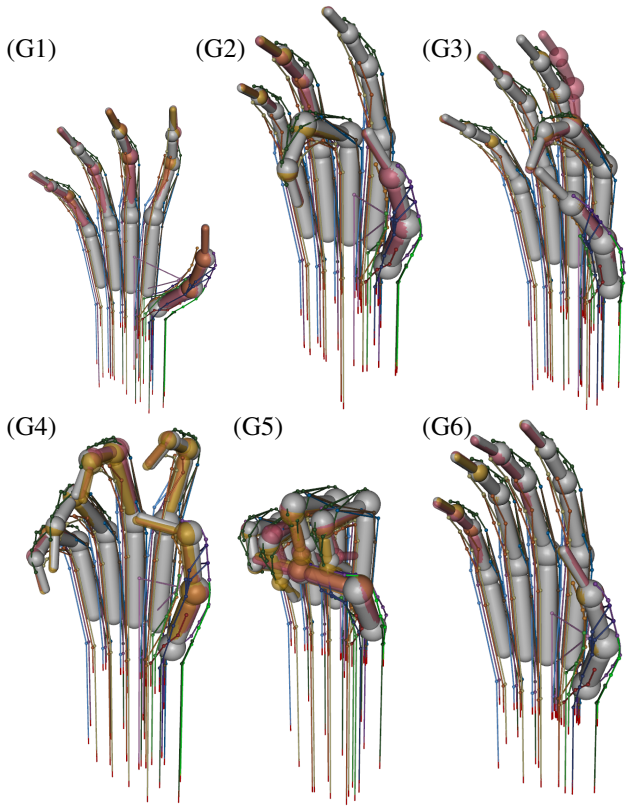

Fig. 3. Desired gestures (red phantom bodies) compared to the gestures achieved (grey bodies) using observer-based control. The observed gestures are illustrated by the yellow phantoms.

controllability and observability characteristics. A further research direction will focus on enhancing both the accuracy of observation and control through various regression and machine learning techniques.

V. Conclusion

This paper addressed the challenge of developing kinematic models to estimate the posture of the Anatomically Correct Biomechatronic Hand model [8] from the measured tendon tension and displacement. The paper highlighted that estimating the joint angles in such complex hand model is challenging due to the increased degrees of freedom in the bone structure, the complexity of the tendon length computations. Although the solution of the nonlinear equations are possible with the efficient gradient-based solvers, the structural controllability of the developed in silico model should be addressed in the future.

Although the solution of the nonlinear equations are possible with the efficient gradient-based solvers, the structural controllability of the developed in silico model should be addressed in the future. This is especially true in the case of hindered movements, when unexpected physical constraint occurs. The uncertainty - inaccuracy experienced along axis Roll suspected to be caused by the given structural properties of the tendon system.

In summary, this article presents a novel approach for joint posture estimation in high-degree-of-freedom anthropomorphic robotic hand models and offers valuable insights into the complexities and challenges associated with achiev-

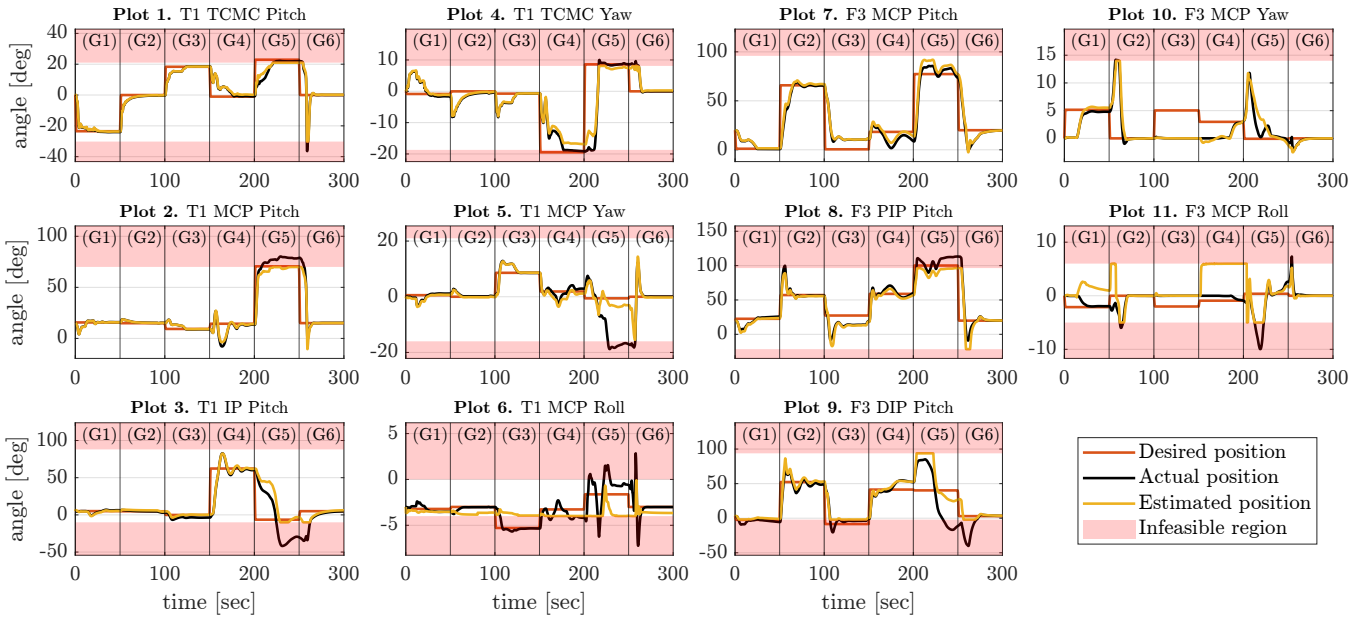

Fig. 4. Results of the posture tracking controller, red lines are the reference, the black illustrate actual angles, the yellow highlight the estimated angles. The labels (G1)–(G6) in the top of each plot highlight the current gesture to be achieved.

ing dexterity and control in such systems. The proposed methodology and the DH description provide a foundation for further research and advancements in the field of robotic hand manipulation and control.

REFERENCES

[1] Z. Xu and E. Todorov, "Design of a highly biomimetic anthropomorphic robotic hand towards artificial limb regeneration," in *2016 IEEE International Conference on Robotics and Automation (ICRA)*, 2016, pp. 3485–3492.

[2] A. A. Mohd Faudzi, J. Ooga, T. Goto, M. Takeichi, and K. Suzumori, "Index finger of a human-like robotic hand using thin soft muscles," *IEEE Robotics and Automation Letters*, vol. 3, no. 1, pp. 92–99, 2018.

[3] R. Konda, D. Bombara, S. Swanbeck, and J. Zhang, "Anthropomorphic twisted string-actuated soft robotic gripper with tendon-based stiffening," *IEEE Transactions on Robotics*, pp. 1–18, 2022.

[4] Z. Zhang, T. Han, J. Pan, and Z. Wang, "Design of anthropomorphic fingers with biomimetic actuation mechanism," *IEEE Robotics and Automation Letters*, vol. 4, no. 4, pp. 3465–3472, 2019.

[5] S. Min and S. Yi, "Development of cable-driven anthropomorphic robot hand," *IEEE Robotics and Automation Letters*, vol. 6, no. 2, pp. 1176–1183, 2021.

[6] A. Shafer and A. D. Deshpande, "Human-like endtip stiffness modulation inspires dexterous manipulation with robotic hands," *IEEE Transactions on Neural Systems and Rehabilitation Engineering*, vol. 30, pp. 1138–1146, 2022.

[7] L. Tian, H. Li, Q. Wang, X. Du, J. Tao, J. S. Chong, N. M. Thalmann, and J. Zheng, "Towards complex and continuous manipulation: a gesture based anthropomorphic robotic hand design," *IEEE Robotics and Automation Letters*, vol. 6, no. 3, pp. 5461–5468, 2021.

[8] B. J. Tasi, M. Koller, and G. Cserey, "Design of the anatomically correct, biomechatronic hand," *arXiv preprint arXiv:1909.07966*, 2019.

[9] D. Huczala, T. Kot, J. Mlotek, J. Suder, and M. Pfurner, "An automated conversion between selected robot kinematic representations," in *2022 10th International Conference on Control, Mechatronics and Automation (ICCMA)*. IEEE, Nov. 2022.

[10] P. K. P. Deepak Ranjan Biswal, "Tendon actuated mechanism based robotic prosthetic hand design for dexterous manipulation and grasping," *Journal of Pharmaceutical Negative Results*, pp. 3089–3106, Dec. 2022.

[11] T. D. Niehues, R. J. King, A. D. Deshpande, and S. Keller, "Development and validation of modeling framework for interconnected tendon networks in robotic and human fingers," May 2017.

[12] F. Lange, G. Quere, and A. Raffin, "Decoupled control of position and / or force of tendon driven fingers," in *2019 International Conference on Robotics and Automation (ICRA)*. IEEE, May 2019.

[13] L. Sievers, J. Pitz, and B. Bäuml, "Learning purely tactile in-hand manipulation with a torque-controlled hand," *arXiv preprint arXiv:2204.03698*, 2022.

[14] T. D. Niehues, "Achieving human-like dexterity in robotic hands: Inspiration from human hand biomechanics and neuromuscular control," Ph.D. dissertation, The University of Texas at Austin, 2017.

[15] P. Esmatloo and A. D. Deshpande, "Fingertip position and force control for dexterous manipulation through model-based control of hand-exoskeleton-environment," in *2020 IEEE/ASME International Conference on Advanced Intelligent Mechatronics (AIM)*. IEEE, Jul. 2020.

[16] Y.-J. Kim, J. Yoon, and Y.-W. Sim, "Fluid lubricated dexterous finger mechanism for human-like impact absorbing capability," *IEEE Robotics and Automation Letters*, vol. 4, no. 4, pp. 3971–3978, 2019.

[17] E. Todorov, T. Erez, and Y. Tassa, "MuJoCo: A physics engine for model-based control," in *2012 IEEE/RSJ International Conference on Intelligent Robots and Systems*. IEEE, Oct. 2012.

[18] J. A. E. Andersson, J. Gillis, G. Horn, J. B. Rawlings, and M. Diehl, "CasADi: A software framework for nonlinear optimization and optimal control," *Mathematical Programming Computation*, vol. 11, no. 1, pp. 1–36, Jul. 2018.

[19] A. Wächter and L. T. Biegler, "On the implementation of an interior-point filter line-search algorithm for large-scale nonlinear programming," *Mathematical Programming*, vol. 106, no. 1, pp. 25–57, Apr. 2005.

[20] P. Amestoy, A. Buttari, J.-Y. L'Excellent, and T. Mary, "Performance and scalability of the block low-rank multifrontal factorization on multicore architectures," *ACM Transactions on Mathematical Software*, vol. 45, pp. 2:1–2:26, 2019.

[21] P. Amestoy, I. S. Duff, J. Koster, and J.-Y. L'Excellent, "A fully asynchronous multifrontal solver using distributed dynamic scheduling," *SIAM Journal on Matrix Analysis and Applications*, vol. 23, no. 1, pp. 15–41, 2001.

[22] OpenAI. (N/A) MuJoCo Documentation. Accessed: 2024-03-25. [Online]. Available: https://mujoco.readthedocs.io/en/stable/modeling.html